CO_2-selective membranes containing amino acid salts for CO_2/N_2 separation

Zhien Zhang [a], Shraavya Rao [a], Yang Han [a], Ruizhi Pang [a], W.S. Winston Ho [a,b,*]

[a] *William G. Lowrie Department of Chemical and Biomolecular Engineering, The Ohio State University, 151 West Woodruff Avenue, Columbus, OH 43210, USA*

[b] *Department of Materials Science and Engineering, The Ohio State University, 2041 College Road, Columbus, OH 43210, USA*

* Corresponding author. Tel.: +1 614 292 9970; fax: +1 614 292 3769.

E-mail address: ho.192@osu.edu (W.S.W. Ho).

Abstract

In this paper, facilitated transport membranes comprising polyvinylamine (PVAm) as fixed carrier and different amino acid salts (AAS) as mobile carriers were synthesized for post-combustion capture. The AAS carriers were prepared by deprotonating alanine (Ala), lysine (Lys), and proline (Pro) with 2-(1-piperazinyl)ethylamine (PZEA). CO_2 separation performances of the membranes with these AAS carriers were compared, and the AAS effectiveness to facilitate transport of CO_2 was in the order of PZEA-Pro > PZEA-Lys > PZEA-Ala. The membrane comprising 35 wt.% PVAm and 65 wt.% PZEA-Pro at 57 °C rendered a promising CO_2 permeance of 936 GPU and a CO_2/N_2 mixed gas selectivity of 193. When the PVAm was reduced to 15 wt.%, i.e., its 20 wt.% was replaced by the mobile carrier of PZEA-Sar (sarcosinate), the permeance further improved to 947 GPU with a remarkable CO_2/N_2 selectivity of 210. Moreover, thermal gravimetric analysis showed a good thermal stability of the membrane, and membrane stability testing also gave stable transport performance. Furthermore, spectroscopic ellipsometry analysis exhibited a uniform membrane selective layer and an excellent agreement on the membrane thickness of *ca.* 170 nm measured independently by SEM. In addition, the membranes presented in this paper surpassed both the Robeson upper bound and the modified upper bound, indicating a great potential for CO_2 capture.

Keywords: Amino acid salt; Facilitated transport membrane; CO_2 capture; Polyvinylamine; Proline

1. Introduction

CO_2 separation and capture from large stationary facilities has attracted attention and interest around the world due to the need to curb greenhouse gases and achieve the target of the global temperature increase below 1.5 °C by 2050 [1–4]. Polymeric membranes have been investigated in the gas separation field, including CO_2 removal, for several decades. Compared with conventional separation methods, advantages of membrane separation are its operation simplicity, small footprint, low energy consumption, and kinetic ability to overcome thermodynamic solubility limitation [2,5]. Many researchers have applied membranes in gas separation processes, showing good performance and potential [6–9].

Facilitated transport membrane (FTM) is based on the reversible reaction between a targeted species and reactive carriers in the membrane, offering both high selectivity and permeability even with a low driving force. As shown in Fig. 1, the carriers are categorized into two types: fixed-site carrier (FSC, green symbol) that is bonded to a polymer chain and possesses limited mobility around its equilibrium chemical-bond position and mobile carrier (red symbol) that moves freely in the membrane. For the FSC, CO_2 reacts with one reactive carrier site and hops to the next; this is commonly termed as the "hopping" mechanism [10]. However, the mobile carrier reacts with CO_2, and their reaction product is also mobile and then diffuses through the membrane. Finally, all the reaction products release CO_2 through the reversible reaction at the membrane-permeate interface to the permeate side. The diffusivity of mobile carrier could reach 10^{-6} cm^2/s when the polymer matrix is fully plasticized by water vapor at 57 °C [11]. Compared to the fixed carrier, the mobile carrier possesses a much higher mobility.

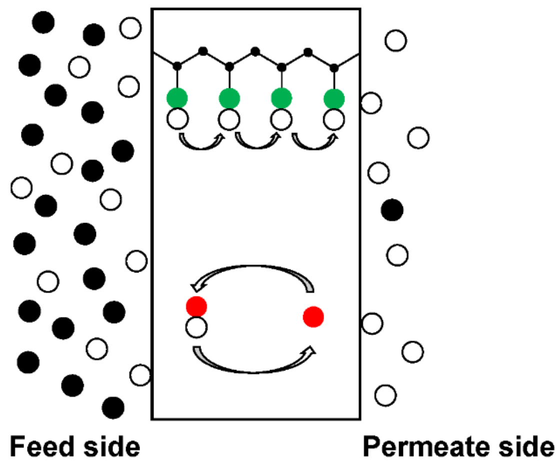

Fig. 1. Schematic representation of the facilitated transport mechanisms.

Among the membranes with reactive carriers, amine-containing FTMs for CO_2 capture have gained much attention [8,12–16]. Generally, reversible reactions between CO_2 and amine could be expressed as follows:

Primary and secondary unhindered amines:

$$2\ R_1R_2NH + CO_2 \rightleftharpoons R_1R_2NH_2^+ + R_1R_2NCO_2^- \qquad (1)$$

Tertiary and hindered amines:

$$R_1R_2R_3N + CO_2 + H_2O \rightleftharpoons R_1R_2\ R_3NH^+ + HCO_3^- \qquad (2)$$

As demonstrated in Eq. (1), 1 mole of CO_2 needs 2 moles of an unhindered amine for the reaction as the resultant carbamate ion is stable [2,5]. A sterically hindered amine is defined as an amine with a primary amino group attached to a tertiary carbon or with a secondary amino group attached to a secondary or tertiary carbon. As illustrated in Eq. (2), a stoichiometric CO_2 loading up to 1 mole of CO_2 per mole of a hindered or tertiary amine is obtained since the carbamate ion formed with the hindered amine is not stable and the tertiary amine does not form a carbamate ion [2,5]. Thus, a hindered amine provides a greater CO_2 loading capacity than an unhindered amine. Moreover, a hindered amine has a better overall CO_2-amine reaction rate than a tertiary amine. Generally, amine carriers with a high CO_2 loading capacity and a good reaction rate are desired. Therefore, a sterically hindered amine is a prominent candidate for the synthesis of CO_2-selective FTMs.

Among the amine carriers, amino acid salts (AAS) have many benefits, including their nonvolatile character and good diffusivity [12,15–19]. Dai et al. fabricated hollow-fiber membranes containing poly(vinyl alcohol) (PVA) and different AAS carriers and tested their CO_2 separation performances [15]. Their results indicated that after adding 40 wt.% potassium prolinate (K-Pro) in the PVA matrix, the permeance of CO_2 increased by 392 GPU (1 GPU = 10^{-6} cm^3(STP) cm^{-2} s^{-1} $cmHg^{-1}$) compared to the pure PVA membrane. However, their composite membranes had a limited selectivity of 35–40 for CO_2 over N_2.

For the purpose of improving the CO_2 loading capacity of the carrier, multi-amines have been used in FTMs [8,13,19,20]. Chen and Ho studied a polyvinylamine (PVAm)/piperazine glycinate (PZ-Gly) membrane, showing a stable and better CO_2 separation performance in comparison with the membranes containing potassium glycinate (K-Gly) or lithium glycinate (Li-Gly) [19]. Recently, Han et al. synthesized an AAS by reacting 2-(1-piperazinyl)ethylamine (PZEA) with sarcosine, and utilized it as the mobile carrier in the PVAm matrix, showing a very good membrane performance [8]. PZEA possesses one primary, one secondary and one tertiary amino groups, which contribute to its good CO_2 loading capacity [21]. Meanwhile, PVAm not only possesses the highest density of amino groups among polyamines for the CO_2 facilitated transport, but also offers a good film forming ability [22]. As illustrated from the literature, it is very important to select the efficient carriers in FTMs to achieve energy-saving and high-performance membranes for CO_2 capture.

In this work, PZEA salts of different amino acids (i.e., alanine, lysine, proline, and sarcosine) were blended and incorporated in a PVAm matrix. The synthesized FTMs were characterized by thermal gravimetric analysis (TGA), Fourier transform infrared spectroscopy (FTIR), scanning electron microscopy (SEM), and spectroscopic ellipsometry. The CO_2 separation performances from a ternary gas mixture ($CO_2/N_2/H_2O$) of the FTMs were investigated at 57 °C, the typical discharge temperature of a coal-derived flue gas [23]. Moreover, the influences of mobile carrier concentration and type in FTMs were studied as well.

2. Experimental

2.1. Materials

PVAm was sourced from Polymin® VX, which was kindly donated by BASF (Vandalia, IL) and purified according to the method presented in our previous publication [8]. The resulting polymer was a poly(*N*-vinylformamide-*co*-vinylamine) (PNVF-*co*-VAm) copolymer with a molecular weight about 2000 kDa. PZEA, 99%, was purchased from Sigma-Aldrich Inc. (St. Louise, MO). Alanine (Ala, 99%), lysine (Lys, 99%), and proline (Pro, 99%) were bought from Alfa Aesar (Ward Hill, MA). Sarcosine (Sar, 98%) was ordered from Acros Organics (Morris Plains, NJ). Potassium bromide (99+% metals basis, FTIR grade) were purchased from Sigma-Aldrich (Milwaukee, WI). Except the PVAm, all chemicals were used without further purification.

A nanoporous polyethersulfone (PES) substrate was fabricated in-house via vapor- and nonsolvent-induced phase inversion, which has been reported in the previous work [24]. The total thickness of the substrate used was *ca.* 120 μm with a nonwoven fabric thickness of *ca.* 95 μm. The PES substrate had a surface porosity of 14.5% and an average pore size of 35 nm [24,25].

Argon and CO_2 gases were ordered from Praxair Inc. (Danbury, CT). N_2 was supplied in house.

2.2. Membrane preparation

The membranes in a thin-film composite configuration were prepared through a knife coating technique. First, the mobile carrier solution was obtained by mixing a 24 wt.% PZEA aqueous solution with an equimolar amount of amino acid. It was stirred under room temperature for 2 h before use. Fig. 2 shows the AAS mobile carriers employed in this work, i.e., PZEA alaninate (PZEA-Ala), PZEA lysinate (PZEA-Lys), PZEA prolinate (PZEA-Pro), and PZEA sarcosinate (PZEA-Sar). The structure of PNVF-*co*-VAm is also depicted in Fig. 2.

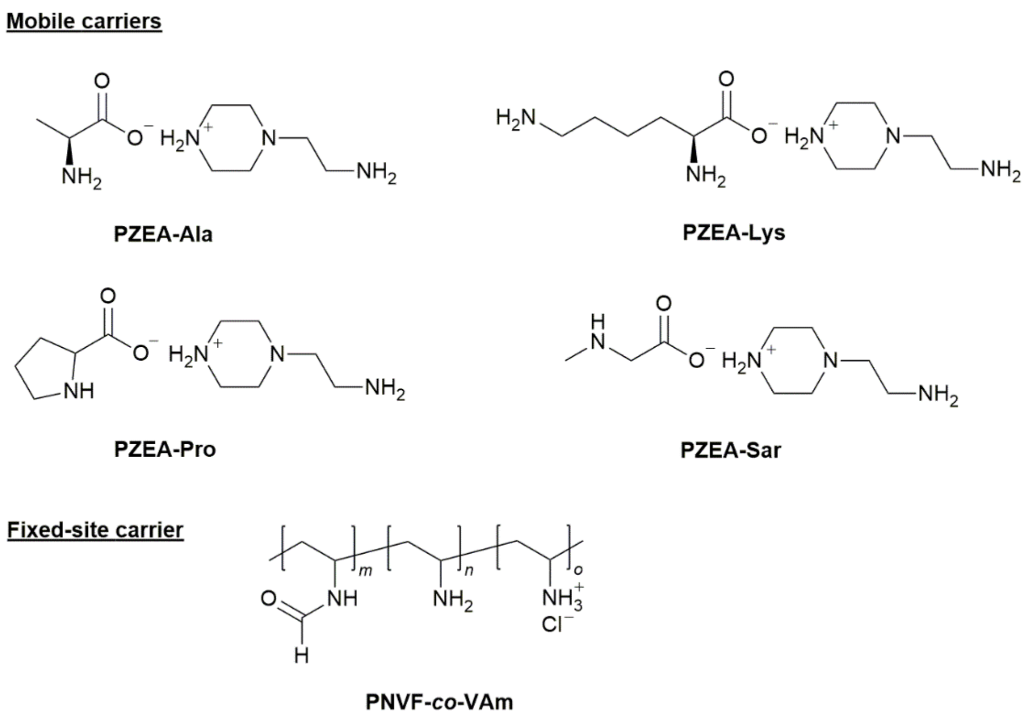

Fig. 2. Chemical structures of carriers used for membrane synthesis.

Next, the coating solution was formed by mixing a 4 wt.% PVAm solution with certain amount of the mobile carrier solution. After stirring for more than 2 h, the solution was centrifuged at 8000 rpm for 3 minutes and coated on the PES support using a GARDCO film applicator with an adjustable gap setting (Paul N. Gardner Co., Pompano Beach, FL). Finally, before the gas permeation test, the resultant membrane was dried inside a fume hood for more than 6 h under room temperature.

2.3. Membrane characterizations

Free-standing films of the selective layer materials were prepared for the thermal and structural analyses. The coating solution was firstly coated on a glass plate, which was dried in a fume hood under ambient conditions overnight to remove most of the water and then in a vacuum oven before the characterization. The dried films had a thickness of ca. 50 μm.

The thermal properties of the membranes were studied using Cahn Thermax 500 high-pressure thermal gravimetric analysis (HPTGA, Thermo Electron Corp., Newington, NH). The HPTGA was equipped with a quartz sample holder (16.8 mm ID, 18.9 mm OD, and 20 mm depth). This HPTGA could be heated up to 600 °C from room temperature at a 10 °C/min heating rate. During the experiment, N_2 was employed as the protective and purge gases with a 150 cc/min flow rate. The sample weight was recorded every second during the experiment. Before the test, the membrane sample was dried at 60 °C overnight inside a vacuum oven to desorb the residual water (Model 29, Thermo Fisher Scientific Inc., Waltham, MA).

The chemical structures of the membranes were characterized by attenuated total reflection (ATR) FTIR spectroscopy using a Nexus 470 Fourier transform infrared spectrometer (Nicolet Instrument Co., Waltham, MA) at room temperature. The spectra were averaged over 32 scans from 650 to 4000 cm^{-1} with a wavenumber resolution of 4 cm^{-1}. Aside from the free standing films, the powdery PZEA-Pro was also characterized. The powder was finely ground and dispersed in KBr and pressed into pellets.

Scanning electron microscopy (SEM, FEI Apreo LoVac, Thermo Fisher Scientific Inc., Waltham, MA) was applied to study the membrane morphology and thickness. The membrane cross-section was prepared by fragile fracture in liquid N_2.

The coating layer thickness of the membrane, i.e., the selective layer, was also obtained with a spectroscopic ellipsometer equipped with an HS-190 rotating analyzer (WVASE 32, J.A. Woollam Co., Lincoln, NE). The two ellipsometry angles, psi (ψ) and delta (Δ), were correlated with the total reflection coefficients [26]:

$$\tan\psi \exp(i\Delta) = \frac{r_\mathrm{p}}{r_\mathrm{s}} = f(\lambda, \phi, n_0, n, l, n_k) \tag{3}$$

where r_p and r_s denote the reflection coefficients of p- and s-polarized lights, respectively, λ the wavelength of the light, ϕ the incidence angle, n_0 the ambient refractive index, n and l the refractive index and the thickness of the coating layer on the substrate, respectively, and n_k the refractive index of the substrate. The correlation function f was adopted from the work by Sirard et al. [26]. The refractive index was a function of the light wavelength by following the Cauchy's dispersion model [27]. Measurements were done on both the bare substrate and the composite membrane for wavelengths from 450 to 1000 nm with 5 nm intervals and reflection angles of 65°, 70°, and 75° to ensure reliability of data interpretation and modeling. Different wavelengths and angles were fit simultaneously in the optical models [26].

2.4. Gas transport measurement

As depicted in Fig. 3, an in-house gas permeation apparatus was employed for testing the mixed gas separation performances of the coated membranes. A membrane sample was placed in a rectangular stainless-steel cell in a temperature-controlled oven (Bemco Inc., Simi Valley, CA). The effective membrane area was 2.7 cm^2 with the feed and sweep operated in a countercurrent pattern. During the test, a 100-cc/min feed gas of 80% N_2 and 20% CO_2 on dry basis and a 30-cc/min sweep gas of pure argon were employed as the feed and sweep gases, respectively. The mass flow controllers (Alicat Scientific Inc., Tucson, AZ) were employed to control their respective flow rates. The pressures of the feed and sweep sides were kept at 1.5 and 1 psig, respectively. Both gas streams were humidified to full saturation with water vapor using their respective stainless-steel bubble column humidifiers (Swagelok Co., Westerville, OH) at a given temperature. The temperatures of the oven and the humidifiers were both controlled at 57 °C (17.2% water vapor content in the gases) that is the typical flue gas temperature exiting the flue gas desulfurization (FGD) unit [23]. Prior to the permeation cell, both saturated feed and sweep gases flowed through their respective dry vessels at 57 °C to remove any entrained water droplets. After knocking out the water vapor in both retentate and permeate sides through their respective condensers, the compositions of the outlet streams were monitored and analyzed using an Agilent 6890 N gas chromatograph (GC, Agilent Technologies, Palo Alto, CA). A thermal conductivity detector (TCD) and a SUPELCO Carboxen® 1004 micropacked GC column (Sigma-Aldrich, St. Louis, MO) were employed in the GC.

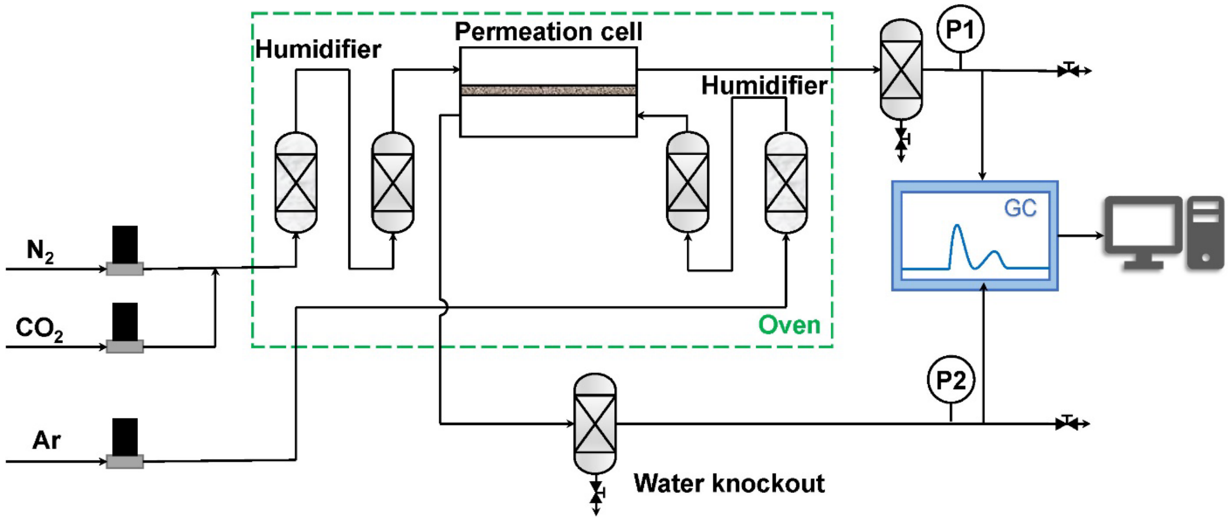

Fig. 3. Schematic of the mixed-gas permeation measurement system.

In order to evaluate the transport results, CO_2 permeance and ideal CO_2/N_2 selectivity for each of the membranes were determined using the following equations, respectively:

$$\frac{P_{CO_2}}{l} = \bar{J}_{CO_2} \frac{\ln\left(\Delta p_{feed,CO_2}/\Delta p_{ret,CO_2}\right)}{\Delta p_{feed,CO_2} - \Delta p_{ret,CO_2}} \tag{4}$$

$$\alpha_{CO_2/N_2} = \frac{P_{CO_2}}{P_{N_2}} \tag{5}$$

where P_{CO_2} and P_{N_2} denote the CO_2 and N_2 permeabilities, respectively, l the effective membrane thickness, $\bar{J}_{CO_2}$ the average CO_2 flux, and $\Delta p_{feed,CO_2}$ and $\Delta p_{ret,CO_2}$ the transmembrane CO_2 partial pressure differentials at the feed inlet and retentate outlet, respectively. In order to determine the ideal selectivity accurately, the stage cut was kept below 2%, at which the ideal selectivity approaches the separation factor. At least three transport measurements were carried out for each membrane under the identical operating conditions.

3. Results and discussion

3.1. Thermal stability characterization

The thermal stability of the membranes can be assessed by TGA analysis. Fig. 4(a) depicts the TGA curves of PZEA, proline and PEZA-Pro, and each curve exhibits a single-step decomposition. The onset of weight loss for PZEA was at 100 °C, indicating a poor thermal stability. However, proline, an amino acid, showed an excellent thermal stability with an onset decomposition temperature of 250 °C. According to the previous work, most of the amino acids have an onset decomposition temperature above 200 °C [15,28]. The PZEA-Pro salt had an onset decomposition temperature of 230 °C, which also exhibited an outstanding thermal stability.

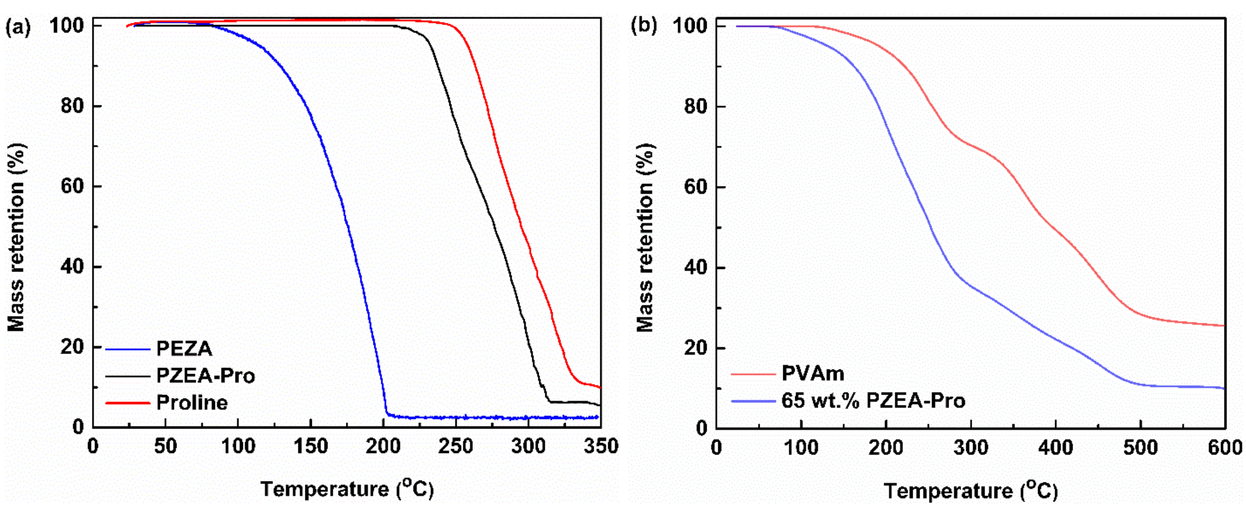

Fig. 4. TGA curves of (a) PZEA, PZEA-Pro, and proline and (b) pure PVAm and a film containing 35 wt.% PVAm and 65 wt.% PEZA-Pro.

Fig. 4(b) compares the thermal properties of pure PVAm and a free-standing film containing 35 wt.% PVAm and 65 wt.% PZEA-Pro. As depicted, PVAm showed a minor and gradual weight loss at 170 °C due to the water evaporation. Afterwards, two main steps of decomposition with onset temperatures at 210 and 340 °C, respectively, were observed, which could be attributed to the release of ammonia and hydrazine from the polymer chain as suggested by the literature [29]. However, as depicted in this figure, the first decomposition of the PVAm/PZEA-Pro film occurred at 105 °C, which was lower than that of pure PVAm. It should be noted that the PVAm/PZEA-Pro sample was extremely hygroscopic, resulting in fast water sorption during sample transfer. Therefore, the early onset of weight loss was due to the desorption of water, which was consistent with the case presented in the literature [30]. It should also be noted that both the PZEA-Pro salt (powdery as shown in Fig. 9) and PVAm (nonhygroscopic amorphous polymer) were nonhygroscopic as evidenced in Fig. 4(a); however, the PVAm/PZEA-Pro sample was observed with extreme hygroscopy.

Similarly, the films of PVAm blended with 65 wt.% PZEA-Lys, 65 wt.% PZEA-Ala, and 65 wt.% PZEA-Pro and 20 wt.% PZEA-Sar also showed no weight loss due to any thermal degradation below 110 °C, as shown in Fig. S1 in the Supporting Information (SI). Based on this thermal stability study, the selective layer materials can meet the requirements for CO_2 capture from flue gas at 57 °C.

3.2. FTIR characterization

Fig. 5 shows the FTIR results of PVAm, PZEA-pro, and the blend thereof with 65 wt.% PZEA-Pro. For PVAm, the bands between 3300 and 3100 cm^{-1} were attributed to the stretching vibrations of primary amine group [19]. The band at 2950 cm^{-1} was associated with the stretching vibration of the C–H bond in the polymer chain. Additionally, the peaks at 1650 and 1585 cm^{-1} corresponded to the C=O stretching and N–H bending of the residual amide group in the PVAm, respectively [19,31]. For the PVAm/PZEA-Pro sample, the intensity of the characteristic peaks associated with the amino groups were significantly enhanced compared to those of pristine PVAm due to the addition of PZEA-Pro. In particular, the presence of the broad band at around 3400 cm^{-1} and the enhanced peak at 1650 cm^{-1} indicated that the incorporation of PZEA-Pro significantly increased the concentration of primary amine groups, corresponding to the 3400 cm^{-1} broad band and the 1650 cm^{-1} peak of PZEA-Pro. The peak at 2980 cm^{-1} was associated with N–H asymmetric stretching, and the band observed at 1410 cm^{-1} was attributed to –COO symmetric stretching [15]. The peak at 1160 cm^{-1} corresponded to the twisting of N–H of the pyrrolidine ring [32]. The PVAm used in this work had a degree of hydrolysis of 15%, hence the addition of PZEA-Pro markedly increased the amine content.

These FTIR results confirmed that the AAS was successfully incorporated into the PVAm matrix. The FTIR results of PVAm blended with PZEA-Lys, PZEA-Ala, and PZEA-Pro/PZEA/Sar are reported in Fig. S2 in the SI.

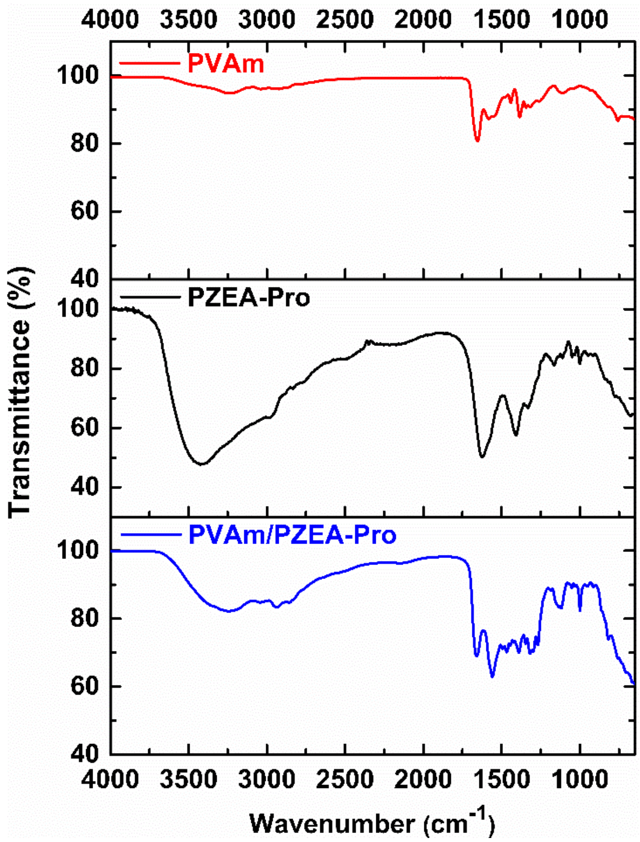

Fig. 5. FTIR spectra of pure PVAm, PZEA-Pro, and the PVAm blended with 65 wt.% PZEA-Pro.

3.3. Membrane morphology

Fig. 6 depicts the cross-section of the composite membrane containing PVAm and PZEA-Pro (at 35/65 wt./wt.) after the gas permeation test. As shown in this figure, the membrane comprised a selective coating layer supported on a porous substrate layer. The selective layer thickness was around 170 nm, which was evenly coated on the PES substrate. This was similar to the membrane of PVAm and PZEA-Sar (at 35/65 wt./wt.) as reported in our previous work [8]. For other membranes in this work, the same gap setting of the coating knife on the PES substrate was employed to ensure the consistent selective layer thickness.

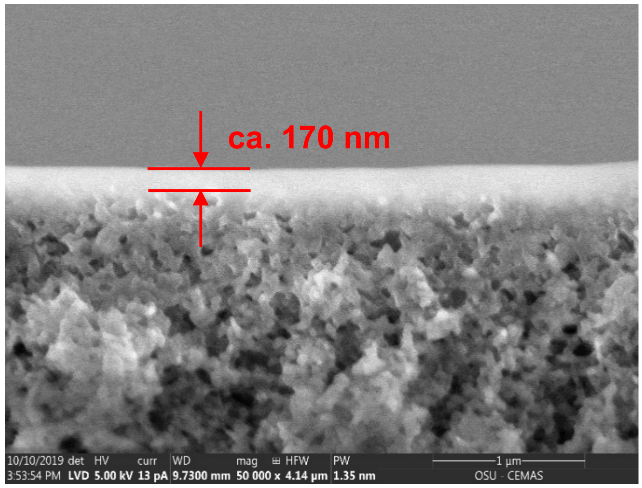

Fig. 6. SEM cross-section image of membrane containing 35 wt.% PVAm and 65 wt.% PZEA-Pro after the gas permeation test.

The thickness and uniformity of the selective layer were also confirmed by spectroscopic ellipsometry. As depicted in Fig. 7, the ellipsometric spectra were fitted by Eq. (3) with the film thickness as the adjustable parameter, rendering a fitted selective layer thickness of 173 nm with a coefficient of determination (R^2) of 98.2%. Therefore, there was an excellent agreement between the spectroscopic ellipsometer measurement and the value measured independently by SEM.

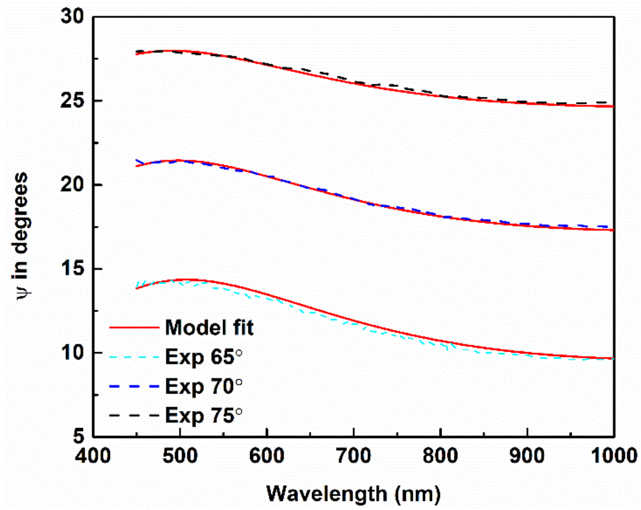

Fig. 7. Experimental ellipsometric spectra and the corresponding model fittings of the composite membrane containing 35 wt.% PVAm and 65 wt.% PZEA-Pro at 25 °C and 1 atm.

3.4. Mixed-gas membrane performances

As found in the previous study [8], the membrane containing PVAm alone showed a CO_2 permeance of 519 GPU with a CO_2/N_2 selectivity of 81. The incorporation of AAS in a membrane could enhance the CO_2/N_2 separation performance due to the mobility enhancement of the mobile carrier and the extra amino groups provided by the AAS for CO_2 reaction [30]. Thus, in this section, we present the enhanced CO_2 separation performances of the PVAm/AAS membranes.

Fig. 8 depicts the transport results of membranes containing different AAS mobile carriers at 57 °C. It should be noted that each data point in this figure was the average of three transport measurements with the error bar shown. As depicted in this figure, the membrane containing 65 wt.% PEZA-Pro had the best transport results of 936 GPU CO_2 permeance and 193 CO_2/N_2 selectivity. In addition, the CO_2 permeance did not increase monotonically with increasing PZEA-

Pro content as opposed to the other AAS carriers. The membranes containing PZEA-Ala, PZEA-Lys, and PZEA-Sar exhibited increasing CO_2 permeances when the AAS contents were increased. However, the membranes containing PZEA-Pro showed the highest CO_2 permeance at 65 wt.% mobile carrier loading, while a further increase in the carrier content led to a reduced permeance and selectivity. The abnormal behavior of PZEA-Pro could be due to the miscibility issue between PVAm and this AAS (as shown in Fig. 9).

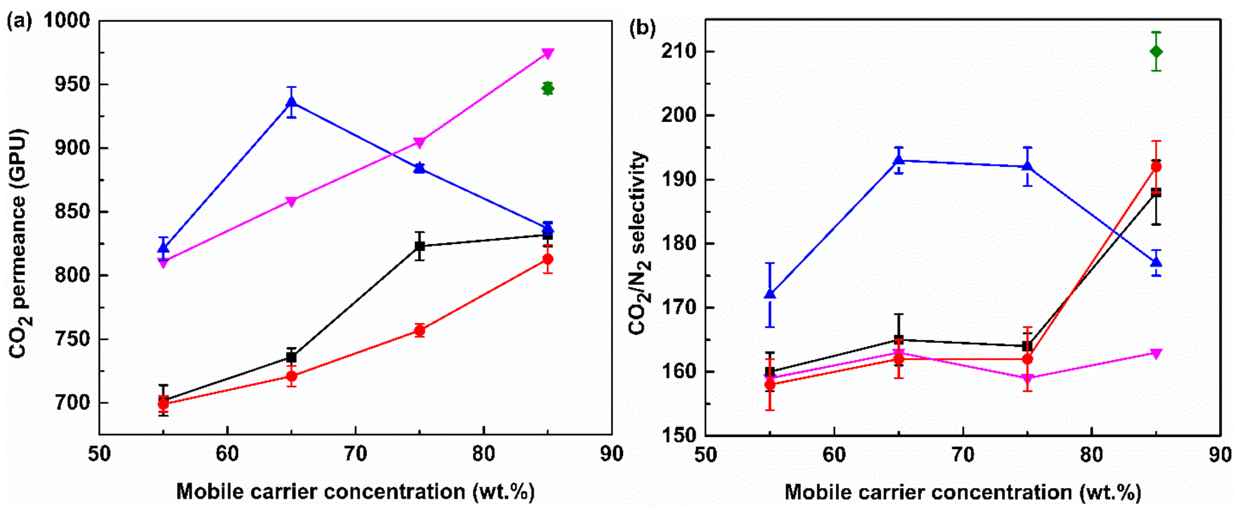

Fig. 8. Comparisons of (a) CO_2 permeances and (b) CO_2/N_2 selectivities of the PVAm membranes with different AAS mobile carrier concentrations at 57 °C. Markers: PZEA-Lys (■); PZEA-Ala (●); PZEA-Pro (▲); PZEA-Sar (▼) [8]; PZEA-Pro/PZEA-Sar (65:20 wt./wt.) (♦).

Fig. 9 displays the photos of the dried films containing various PZEA-Pro contents (0, 25, 45, 65 and 85 wt.%) and the PZEA-Pro salt. As shown, the pure PVAm rendered a transparent film. When the PZEA-Pro content was less than or equal to 65 wt.%, the film was still homogeneous.

However, the film containing 85 wt.% PEZA-Pro showed salt on the surface, indicating phase separation. This might account for the poor transport results when using 85 wt.% PZEA-Pro as the mobile carrier (837 GPU CO_2 permeance and 177 CO_2/N_2 selectivity) compared to the membrane containing 65 wt.% PZEA-Pro. Dai et al. also found that a high content of K-Pro in the FTM caused a negative influence on the CO_2 capture performance owing to the micelle formation and aggregation in the coating solution [15]. The last photo (bottom, right) in this figure shows the appearance of the PZEA-Pro salt, where the dark grey spots were the uncovered petri dish as a result of drying this salt.

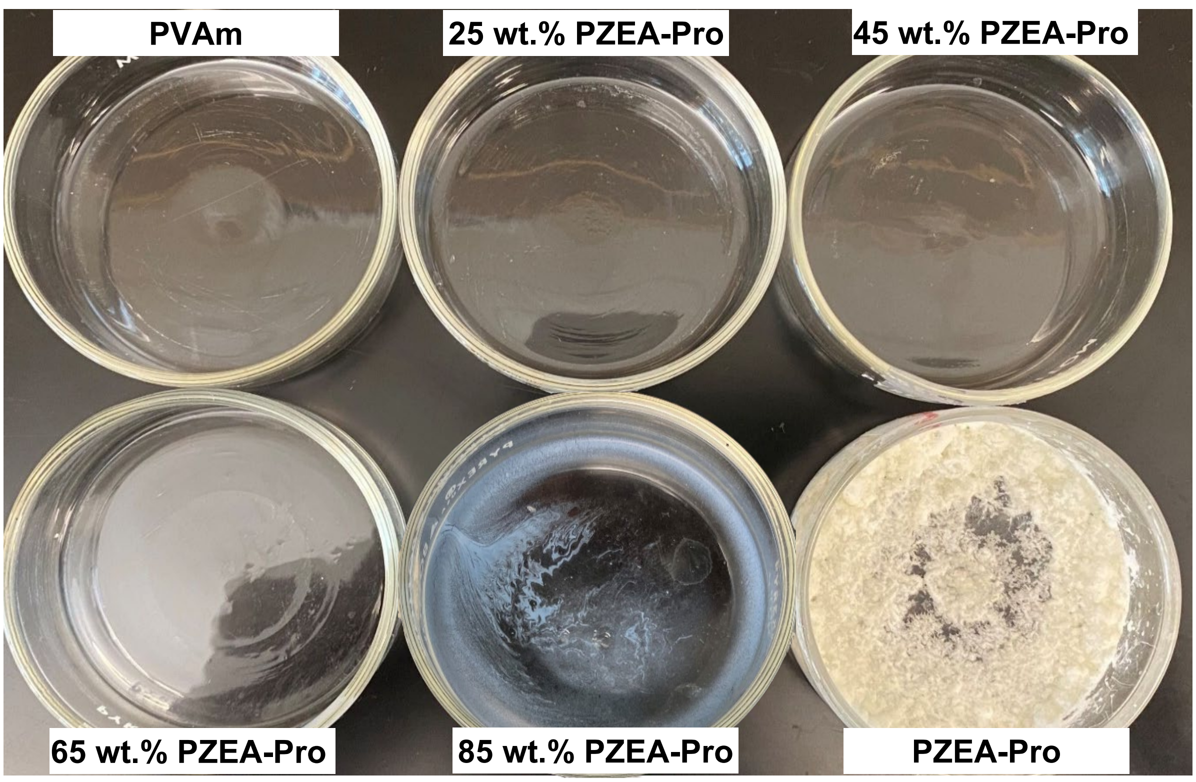

Fig. 9. Photos of dried films of PVAm with various contents of PZEA-Pro and the PZEA-Pro salt.

Compared to the membrane using PZEA-Pro as the mobile carrier, the membranes containing PZEA-Ala or PZEA-Lys showed worse CO_2 transport performances. The PVAm/PZEA-Ala membrane exhibited a CO_2 permeance of only 813 GPU at 85 wt.% loading, which was due to the lowest reactivity towards CO_2 in comparison with other mobile carriers. The reaction rate constant between CO_2 and alaninate salt was reported to be lower than those of lysinate and prolinate, which was partially evidenced by the lower pK_a of the α-ammonium ion on alaninate, i.e., 9.87 vs. 10.53 and 10.64 for the counterparts on lysinate and prolinate, respectively [33].

Furthermore, the PVAm/PZEA-Lys membrane rendered a CO_2 permeance of 832 GPU at 85 wt.% mobile carrier loading, which was in between PVAm/PZEA-Ala and PVAm/PZEA-Pro membranes. This was because the lysinate salt had a lower CO_2 reaction rate constant than the prolinate salt. The pK_a value of the amino group in prolinate was 10.64, which was higher than those of lysinate (10.53 and 8.95 for the α- and side chain-ammonium ions, respectively) [34]. Thus, prolinate was more reactive to CO_2 than lysinate. All the CO_2/N_2 selectivities of the membranes were between 155 – 200, indicating that these membranes were capable of highly-selective separation of CO_2 over N_2. The influence of the amine concentration in these membranes is reported in Fig. S3 in the SI, showing that the amine concentration was not a strong predictor of the membrane transport performance.

In order to further improve the transport results of the PVAm/PZEA-Pro membrane, PZEA-Sar was added into the coating solution. This was based on the high miscibility of PZEA-Sar with PVAm [8] and the highest CO_2 permeance of the membrane containing 85 wt.% PZEA-Sar shown in Fig. 8. On the other hand, other two mobile carriers (PZEA-Lys and PZEA-Ala) exhibited much worse transport performance compared with PZEA-Sar. Thus, we chose PZEA-Sar as the second mobile carrier in the FTMs.

Table 1 lists the transport results of the membranes containing different ratios of PVAm, PZEA-Pro, and PZEA-Sar. All three membranes listed in this table had a better separation performance compared to the membranes with PZEA-Pro as the only mobile carrier. Specially, the membrane containing 15 wt.% PVAm, 65 wt.% PZEA-Pro, and 20 wt.% PZEA-Sar was homogeneous and did not show any inhomogeneity as opposed to the counterpart containing 85 wt.% PZEA-Pro. This homogeneous membrane exhibited a 947 GPU CO_2 permeance, which was slightly higher than that (936 GPU) of the membrane containing 35 wt.% PVAm and 65 wt.% PZEA-Pro. More importantly, the former had an excellent CO_2/N_2 selectivity of 210, which was much better than that (193) of the latter. These permeance and selectivity results of this membrane are also illustrated in Fig. 8 for comparison. In this case, the greater content of mobile carriers enhanced the permeance and selectivity. As shown in Fig. 8, although the PVAm and PZEA-Sar (at 15/85 wt./wt.) membrane showed a higher permeance than the PVAm/PZEA-Pro/PZEA-Sar (15/65/20 by weight) membrane, the former had a lower selectivity than the latter as the former had a higher N_2 permeance.

Table 1. CO_2/N_2 separation performances of membranes containing various ratios of PVAm/PZEA-Pro/PZEA-Sar.

PVAm/PZEA-Pro/PZEA-Sar (by wt.)	CO_2 permeance (GPU)	CO_2/N_2 selectivity
15/55/30	830	171
15/65/20	947	210
15/75/10	892	174

In addition, as demonstrated in Table 1, this PVAm/PZEA-Pro/PZEA-Sar (15/65/20 by weight) membrane exhibited a superior transport performance than other two membranes. The PVAm/PZEA-Pro/PZEA-Sar (15/55/30 by weight) membrane showed a lower CO_2 permeance of 830 GPU, which was due to the lower PZEA-Pro content. The PVAm/PZEA-Pro/PZEA-Sar (15/75/10 by weight) membrane rendered a worse transport performance than the PVAm/PZEA-Pro/PZEA-Sar (15/65/20 by weight) membrane. This was due to the phase separation issue when the content of PZEA-Pro in the membrane was excessively high as mentioned earlier.

3.5. Membrane stability

Fig. 10 presents the stability performance of the membrane of 15 wt.% PVAm, 65 wt.% PZEA-Pro, and 20 wt.% PZEA-Sar. The membrane exhibited an average CO_2 permeance of 926 GPU and a CO_2/N_2 selectivity of 204. Also, this membrane had a stable CO_2 separation performance for 110 h at 57 °C. There was no reduction in both CO_2 permeance and CO_2/N_2 selectivity during the test. In our previous work [18], the spiral-wound module using PVAm/PZEA-Sar membrane has shown a 500-h stable performance with actual flue gas at the National Carbon Capture Center. It should be noted that a careful water management is needed to prevent accidental water condensation in the membrane module for a prolonged period of time. The good stability of this membrane shows the promise for the industrial application.

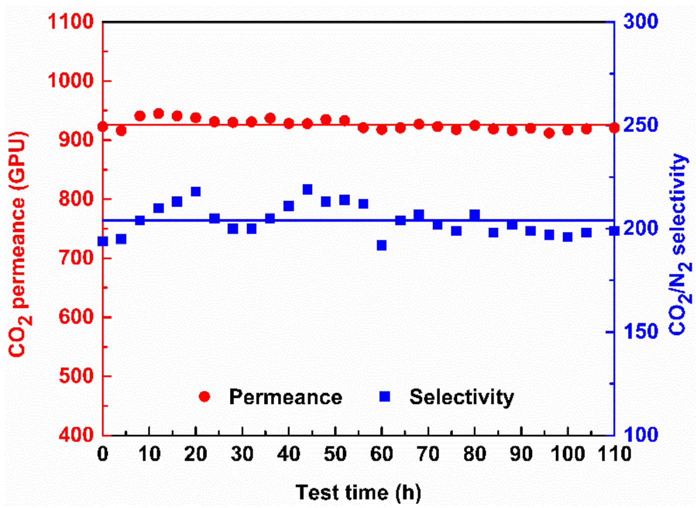

Fig. 10. Stability of a FTM containing 65 wt.% PZEA-Pro, 20 wt.% PZEA-Sar, and 15 wt.% PVAm for a 110 h at 57 °C.

3.6. Performance comparison of membranes containing various amino acid salts

Table 2 compares the CO_2/N_2 separation performances of the AAS-containing membranes in this work with those reported in the literature. First, for different AAS carriers deprotonated by PZEA, the PVAm/PZEA-Sar membrane [8] exhibited a slightly better CO_2 permeance than the PVAm/PZEA-Pro membrane at the same mobile carrier content. This can be explained by the fact that sarcosinate has a methyl group attached to the amino group to become a hindered amine, which provides a greater CO_2 loading capacity [8]. The membrane with PZEA-Gly as the mobile carrier [8] showed a lower permeance compared to those with PZEA-Sar or PZEA-Pro, which could be explained by the lower reactivity of glycinate compared with prolinate and sarcosinate [35].

Table 2. Comparison of the transport performance of various amino acid salt-containing membranes.

Membrane	T (°C)	p_{CO_2} (atm) [a]	ℓ (μm) [b]	CO_2 permeance (GPU)	CO_2/N_2 selectivity	Ref.
PVAm/PZEA-Pro/PZEA-Sar	57	0.166	0.17	947	210	This work
PVAm/PZEA-Pro	57	0.166	0.17	936	193	This work
PVAm/PZEA-Ala	57	0.166	0.17	813	192	This work
PVAm/PZEA-Lys	57	0.166	0.17	832	188	This work
PVAm/PZEA-Gly	57	0.166	0.17	911	163	[8]
	57	0.166	0.17	975	155	[8]
PVAm/PZEA-Sar	67	0.731	0.17	1450	165	[36]
	77	0.708	0.17	2100	119	[36]
PVAm/PZ-Gly	57	0.166	0.17	839	161	[8]
	57	0.166	0.1	1100	210	[13]
PVAm/Li-Gly	57	0.166	0.1	1010	202	[13]
PVAm/K-Gly	57	0.166	0.1	903	173	[13]
PVA/sterically hindered polyallylamine/PZEA-Sar	35	1.48	0.1 – 0.3	652	41	[37]
PVA/sterically hindered polyallylamine/K-Pro	35	1.48	0.2	730	31	[38]
PVA/K-Pro	22	0.197	0.5	793	40	[15]
PVA/K-Gly	22	0.197	0.5	640	32	[15]
PVA/K-Cys	22	0.197	0.5	650	36	[15]
PVA/K arginate (K-Arg)	22	0.098	0.5	661	34	[15]
Pebax®/Na-Gly	25	0.197	75 – 100	1023 Barrers [c]	91	[17]

[a] CO_2 partial pressure.

[b] Selective layer thickness.

[c] Only CO_2 permeability is reported.

The cation effect is also demonstrated in Table 2 by a series of AAS carriers containing glycinate but with different cations. If the PZEA cation was replaced by the PZ cation, the CO_2 permeance of the PVAm/PZ-Gly membrane was slightly lower than that of the PVAm/PZEA-Gly membrane [8]. This might be due to the higher CO_2 loading capacity of PZEA, which contains 3 amino groups, i.e., primary, secondary and tertiary amino groups in comparison with PZ with 2 amino groups [8]. For the AAS carriers deprotonated by LiOH and KOH [13], these membranes had a lower CO_2 permeance compared with those using PZ or PZEA as the base [8]. For instance, Li-Gly and K-Gly had a poorer performance due to the lack of amino group on the cation, which weakened the facilitated transport of CO_2. Additionally, the PVAm/Li-Gly membrane showed a higher CO_2 permeance (1010 GPU) than the PVAm/K-Gly membrane (903 GPU). This was because Li-Gly had a smaller molecular weight than K-Gly, and hence it provided more moles of amino groups for the reaction at the same mobile carrier weight. Also, Li-Gly exhibited a higher diffusivity because of the smaller molecular size compared to K-Gly [13].

For the membranes containing PVA and various AAS carriers, the CO_2 permeance of potassium cysteinate (K-Cys) was worse than K-Pro but better than K-Gly under the same conditions [15]. This was probably because cysteinate had a pK_a of 10.4 for the α-ammonium ion, which was lower than that of prolinate (10.64) but higher than that of glycinate (9.78 for the α-ammonium ion) [33]. Compared with membranes using PVAm as the fixed-site carrier, these PVA-containing membranes showed lower CO_2 permeances because of the absence of amino groups.

The effect of operating temperature is also demonstrated in Table 2 by the PVAm/PZEA-Sar membrane, the CO_2 permeance of which increased by 1125 GPU with increasing temperature from 57 to 77 °C [8,36]. However, the CO_2/N_2 selectivity reduced from 155 to 119. The increased CO_2 permeance with increasing temperature was primarily attributed to the faster CO_2-amine reaction [19,36]. In addition, the gas diffusion through the membrane was a thermally activated process. The higher CO_2 diffusivity at a higher temperature also improved the CO_2 permeance. However, CO_2 had a much lower activation energy than that of N_2 [39]. Thus, a higher operating temperature promoted the diffusion of N_2 more prominently. Therefore, the CO_2 selectivity over N_2 reduced with increasing temperature. The effect of temperature on the membranes containing PZEA-Pro should be studied in the future.

Lastly, a thinner selective layer of the composite membrane had a positive impact on the CO_2 permeance. It was noted that the PVAm/PZ-Gly membrane with a selective layer thickness of 100 nm exhibited a CO_2 permeance that was 261 GPU higher than that with a 170-nm thick selective layer. The effect of selective layer thickness should also be studied for the membranes containing PZEA-Pro.

3.7. Comparison of membrane performances with solution-diffusion membranes

A trade-off between permeance and selectivity is a commonly observed phenomenon in polymeric membranes based on the solution-diffusion mechanism [40]. Fig. 11 presents the CO_2/N_2 selectivities and CO_2 permeances of the FTMs in this work versus the 2008 Robeson upper bound [41] and the 2019 revised upper bound [42]. In both upper bounds, the permeability values were converted to the permeances by assuming a membrane thickness of 170 nm, which was the same as the selective layer thickness of the composite membranes in this study. The permeance was used here since the permeability of a FTM is dependent on its thickness, and the permeability of a thick free-standing film cannot be used to extrapolate the permeance of a thin FTM [43]. All the membranes containing AAS mobile carriers surpassed both upper bounds, indicating superior CO_2/N_2 separation performances. Thus, both the permeance and selectivity were dramatically improved by the addition of AAS mobile carriers.

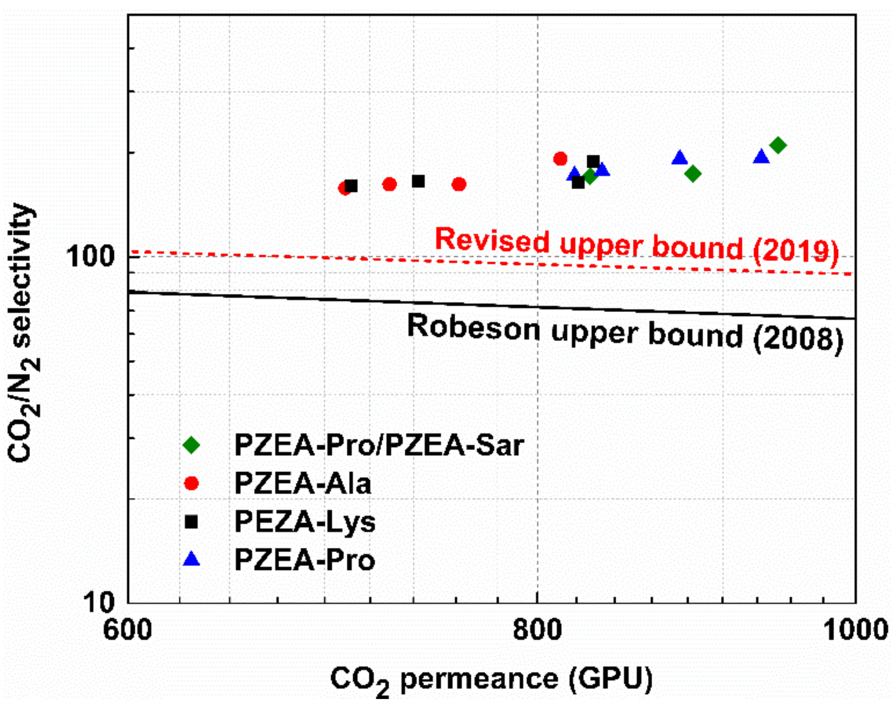

Fig. 11. CO_2/N_2 separation performances of the FTMs in this work vs. the 2008 Robeson upper bound [41] and the 2019 revised upper bound [42] assuming a membrane thickness of 170 nm.

4. Conclusions

In this study, FTMs using PVAm as the fixed-site carrier and different AAS mobile carriers were synthesized, and their CO_2/N_2 transport results were investigated. The AAS effectiveness to facilitate CO_2 transport was in the order of PZEA-Pro > PZEA-Lys > PZEA-Ala. The synthesized membrane containing PVAm and PZEA-Pro (at 35/65 wt./wt.) exhibited a promising CO_2 permeance of 936 GPU with a 193 selectivity for CO_2 over N_2 at 57 °C. As the PVAm was reduced to 15 wt.%, i.e., its 20 wt.% was replaced by PZEA-Sar, the permeance further increased to 947 GPU with an excellent CO_2/N_2 selectivity of 210. This membrane also showed stable transport results for 110 h. Moreover, thermal gravimetric analysis indicated a good thermal stability of the membrane and the AAS of PEZA-Pro with a better thermal stability than the PZEA alone. Furthermore, the spectroscopic ellipsometry analysis exhibited a uniform selective layer of the membrane, and it also exhibited an excellent agreement on the membrane thickness of *ca.* 170 nm measured independently by SEM. Finally, the membranes presented in this work showed promising transport results and surpassed both the Robeson upper bound and the revised upper bound, indicating a great potential for CO_2 capture.

Acknowledgments

The authors would like to thank Isaac A. Aurelio, José D. Figueroa, Krista Hill and David A. Lang of the U.S. Department of Energy – National Energy Technology Laboratory (DOE-NETL) and Matthew Usher, Dean Bell, and Randy Keefer of American Electric Power (AEP) Engineering Services for their invaluable inputs. We are thankful to the donations of Ultrason® E7020P PES and Polymin® VX from BASF Corporation (Charlotte, NC) and Purolite® A600OH resins from Purolite Corporation (Bala Cynwyd, PA), respectively. SEM was carried out at the Center for Electron Microscopy and Analysis (CEMAS) at The Ohio State University. The authors would like to acknowledge DOE-NETL (DE-FE0026919 and DE-FE0031731) and the Ohio Development Services Agency (OER-CDO-D-15-09 and OER-CDO-D-19-12) for the financial support of this work. This research was partially supported by the Department of Energy (DE-FE0026919 and DE-FE0031731) with substantial involvement of the NETL, Pittsburgh, PA, USA.

Nomenclature

Symbols

$\bar{J}_{\mathrm{CO_2}}$	average CO_2 flux
l	effective membrane thickness
n	refractive index of the coating layer
n_0	ambient refractive index
n_{k}	refractive index of the substrate
$P_{\mathrm{CO_2}}$	CO_2 permeability
$P_{\mathrm{N_2}}$	N_2 permeability
$\Delta p_{\mathrm{feed,CO_2}}$	partial pressure differential of CO_2 at the feed inlet
$\Delta p_{\mathrm{ret,CO_2}}$	partial pressure differential of CO_2 at the retentate outlet
r_{p}	reflection coefficient of p-polarized light
r_{s}	reflection coefficient of s-polarized light

Greek letters

Δ	ellipsometric angle delta
α	selectivity
λ	wavelength of the light
ϕ	incidence angle
ψ	ellipsometric angle psi

References

[1] P.G. Boyd, A. Chidambaram, E. García-Díez, C.P. Ireland, T.D. Daff, R. Bounds, A. Gładysiak, P. Schouwink, S.M. Moosavi, M. Mercedes Maroto-Valer, J.A. Reimer, J.A.R. Navarro, T.K. Woo, S. Garcia, K.C. Stylianou, B. Smit, Data-driven design of metal-organic frameworks for wet flue gas CO_2 capture, Nature 576 (2019) 253–256. doi:10.1038/s41586-019-1798-7.

[2] Y. Han, W.S.W. Ho, Recent advances in polymeric membranes for CO_2 capture, Chinese J. Chem. Eng. 26 (2018) 2238–2254. doi:10.1016/j.cjche.2018.07.010.

[3] J. Yan, Z. Zhang, Carbon Capture, Utilization and Storage (CCUS), Appl. Energy 235 (2019) 1289–1299. doi:10.1016/j.apenergy.2018.11.019.

[4] V. Masson-Delmotte, P. Zhai, H.-O. Pörtner, D. Roberts, J. Skea, P.R. Shukla, A. Pirani, W. Moufouma-Okia, C. Péan, R. Pidcock, Global warming of 1.5 °C. An IPCC Special Report on the impacts of global warming of 1.5°C above pre-industrial levels and related global greenhouse gas emission pathways, in the context of strengthening the global response to the threat of climate change, 2018. www.ipcc.ch/sr15/ (accessed April 18, 2021).

[5] Y. Han, W.S.W. Ho, Recent developments on polymeric membranes for CO_2 capture from flue gas, J. Polym. Eng. 40 (2020) 529–542. doi:10.1515/polyeng-2019-0298.

[6] K. Xie, Q. Fu, G.G. Qiao, P.A. Webley, Recent progress on fabrication methods of polymeric thin film gas separation membranes for CO_2 capture, J. Membr. Sci. 572 (2019)

38–60. doi:10.1016/j.memsci.2018.10.049.

[7] U.W.R. Siagian, A. Raksajati, N.F. Himma, K. Khoiruddin, I.G. Wenten, Membrane-based carbon capture technologies: Membrane gas separation vs. membrane contactor, J. Nat. Gas Sci. Eng. 67 (2019) 172–195. doi:10.1016/j.jngse.2019.04.008.

[8] Y. Han, D. Wu, W.S.W. Ho, Nanotube-reinforced facilitated transport membrane for CO_2/N_2 separation with vacuum operation, J. Membr. Sci. 567 (2018) 261–271. doi:10.1016/j.memsci.2018.08.061.

[9] L. Ansaloni, A. Hartono, M. Awais, H.K. Knuutila, L. Deng, CO_2 capture using highly viscous amine blends in non-porous membrane contactors, Chem. Eng. J. 359 (2019) 1581–1591. doi:10.1016/j.cej.2018.11.014.

[10] E.L. Cussler, R. Aris, A. Bhown, On the limits of facilitated diffusion, J. Membr. Sci. 43 (1989) 149–164. doi:10.1016/0362-546X(81)90091-2.

[11] X. Deng, C. Zou, Y. Han, L.-C. Lin, W.S.W. Ho, Computational evaluation of carriers in facilitated transport membranes for postcombustion carbon capture, J. Phys. Chem. C 124 (2020) 25322–25330. doi:10.1021/acs.jpcc.0c07627.

[12] J. Zou, W.S.W. Ho, CO_2-selective polymeric membranes containing amines in crosslinked poly(vinyl alcohol), J. Membr. Sci. 286 (2006) 310–321. doi:10.1016/j.memsci.2006.10.013.

[13] Y. Chen, L. Zhao, B. Wang, P. Dutta, W.S.W. Ho, Amine-containing polymer/zeolite Y composite membranes for CO_2/N_2 separation, J. Membr. Sci. 497 (2016) 21–28.

doi:10.1016/j.memsci.2015.09.036.

[14] A. Mondal, M. Barooah, B. Mandal, Effect of single and blended amine carriers on CO_2 separation from CO_2/N_2 mixtures using crosslinked thin-film poly(vinyl alcohol) composite membrane, Int. J. Greenh. Gas Con. 39 (2015) 27–38. doi:10.1016/j.ijggc.2015.05.002.

[15] Z. Dai, J. Deng, L. Ansaloni, S. Janakiram, L. Deng, Thin-film-composite hollow fiber membranes containing amino acid salts as mobile carriers for CO_2 separation, J. Membr. Sci. 578 (2019) 61–68. doi:10.1016/j.memsci.2019.02.023.

[16] B. Dhuiège, E. Lasseuguette, M.C. Brochier-Salon, M.C. Ferrari, K. Missoum, Crosslinked facilitated transport membranes based on carboxymethylated NFC and amine-based fixed carriers for carbon capture, utilization, and storage applications, Appl. Sci. 10 (2020) 414. doi:10.3390/app10010414.

[17] H. Zhang, H. Tian, J. Zhang, R. Guo, X. Li, Facilitated transport membranes with an amino acid salt for highly efficient CO_2 separation, Int. J. Greenh. Gas Con. 78 (2018) 85–93. doi:10.1016/j.ijggc.2018.07.014.

[18] Y. Han, W. Salim, K.K. Chen, D. Wu, W.S.W. Ho, Field trial of spiral-wound facilitated transport membrane module for CO_2 capture from flue gas, J. Membr. Sci. 575 (2019) 242–251. doi:10.1016/j.memsci.2019.01.024.

[19] Y. Chen, W.S.W. Ho, High-molecular-weight polyvinylamine/piperazine glycinate membranes for CO_2 capture from flue gas, J. Membr. Sci. 514 (2016) 376–384. doi:10.1016/j.memsci.2016.05.005.

[20] S. Yuan, Z. Wang, Z. Qiao, M. Wang, J. Wang, S. Wang, Improvement of CO_2/N_2 separation characteristics of polyvinylamine by modifying with ethylenediamine, J. Membr. Sci. 378 (2011) 425–437. doi:10.1016/j.memsci.2011.05.023.

[21] S. Paul, A.K. Ghoshal, B. Mandal, Kinetics of absorption of carbon dioxide into aqueous solution of 2-(1-piperazinyl)-ethylamine, Chem. Eng. Sci. 64 (2009) 313–321. doi:10.1016/j.ces.2008.10.025.

[22] R. Pelton, Polyvinylamine: A tool for engineering interfaces, Langmuir 30 (2014) 15373–15382. doi:10.1021/la5017214.

[23] V. Chou, H. Goldstein, E. Lewis, M.C. Woods, Eliminating the Derate of Carbon Capture Retrofits Final Report, 2011. www.netl.doe.gov (accessed May 11, 2020).

[24] D. Wu, L. Zhao, V.K. Vakharia, W. Salim, W.S.W. Ho, Synthesis and characterization of nanoporous polyethersulfone membrane as support for composite membrane in CO_2 separation: From lab to pilot scale, J. Membr. Sci. 510 (2016) 58–71. doi:10.1016/j.memsci.2016.03.022.

[25] R. Pang, K.K. Chen, Y. Han, W.S.W. Ho, Highly permeable polyethersulfone substrates with bicontinuous structure for composite membranes in CO_2/N_2 separation, J. Membr. Sci. 612 (2020) 118443. doi:10.1016/j.memsci.2020.118443.

[26] S.M. Sirard, P.F. Green, K.P. Johnston, Spectroscopic ellipsometry investigation of the swelling of poly(dimethylsiloxane) thin films with high pressure carbon dioxide, J. Phys. Chem. B 105 (2001) 766–772. doi:10.1021/jp002592d.

[27] J.D. Wind, S.M. Sirard, D.R. Paul, P.F. Green, K.P. Johnston, W.J. Koros, Carbon dioxide-induced plasticization of polyimide membranes: Pseudo-equilibrium relationships of diffusion, sorption, and swelling, Macromolecules 36 (2003) 6433–6441. doi:10.1021/ma0343582.

[28] F. Rodante, Thermodynamics and kinetics of decomposition processes for standard α-amino acids and some of their dipeptides in the solid state, Thermochim. Acta. 200 (1992) 47–61. doi:10.1016/0040-6031(92)85105-5.

[29] R. Casadei, D. Venturi, M.G. Baschetti, L. Giorgini, E. Maccaferri, S. Ligi, Polyvinylamine membranes containing graphene-based nanofillers for carbon capture applications, Membranes 9 (2019) 119. doi:10.3390/membranes9090119.

[30] Y. Qin, J. Lv, X. Fu, R. Guo, X. Li, J. Zhang, Z. Wei, High-performance SPEEK/amino acid salt membranes for CO_2 separation, RSC Adv. 6 (2016) 2252–2258. doi:10.1039/c5ra25089g.

[31] J. Wu, Z. Wang, Y. Wang, W. Yan, J. Wang, S. Wang, Polyvinylamine-grafted polyamide reverse osmosis membrane with improved antifouling property, J. Membr. Sci. 495 (2015) 1–13. doi:10.1016/j.memsci.2015.08.007.

[32] G.K. Kharmawlong, R. Nongrum, B. Chhetri, J.W.S. Rani, N. Rahman, A.K. Yadav, R. Nongkhlaw, Green and efficient one-pot synthesis of 2,3-dihydroquinazolin-4(1*H*)-ones and their anthelmintic studies, Synth. Commun. 49 (2019) 2683–2695. doi:10.1080/00397911.2019.1639754.

[33] A.F. Ciftja, A. Hartono, H.F. Svendsen, Selection of amine amino acids salt systems for CO_2 capture, Energy Procedia 37 (2013) 1597–1604. doi:10.1016/j.egypro.2013.06.035.

[34] S. Shen, Y.N. Yang, Y. Bian, Y. Zhao, Kinetics of CO_2 absorption into aqueous basic amino acid salt: potassium salt of lysine solution, Env. Sci Technol. 50 (2016) 2054–2063. doi:10.1021/acs.est.5b04515.

[35] H. Thee, N.J. Nicholas, K.H. Smith, G. da Silva, S.E. Kentish, G.W. Stevens, A kinetic study of CO_2 capture with potassium carbonate solutions promoted with various amino acids: Glycine, sarcosine and proline, Int. J. Greenh. Gas Con. 20 (2014) 2120–2222. doi:10.1016/j.ijggc.2013.10.027.

[36] Y. Han, D. Wu, W.S.W. Ho, Simultaneous effects of temperature and vacuum and feed pressures on facilitated transport membrane for CO_2/N_2 separation, J. Membr. Sci. 573 (2019) 476–484. doi:S0376738818325602.

[37] S. Janakiram, X. Yu, L. Ansaloni, Z. Dai, L. Deng, Manipulation of fibril surfaces in nanocellulose-based facilitated transport membranes for enhanced CO_2 capture, ACS Appl. Mater. Interfaces 11 (2019) 33302–33313. doi:10.1021/acsami.9b09920.

[38] S. Janakiram, J.L. Martín Espejo, K.K. Høisæter, A. Lindbråthen, L. Ansaloni, L. Deng, Three-phase hybrid facilitated transport hollow fiber membranes for enhanced CO_2 separation, Appl. Mater. Today 21 (2020) 100801. doi:10.1016/j.apmt.2020.100801.

[39] Y. Han, W.S.W. Ho, Recent advances in polymeric facilitated transport membranes for carbon dioxide separation and hydrogen purification, J. Polym. Sci. 58 (2020) 2435–2449.

doi:10.1002/pol.20200187.

[40] H.B. Park, J. Kamcev, L.M. Robeson, M. Elimelech, B.D. Freeman, Maximizing the right stuff: The trade-off between membrane permeability and selectivity, Science 356 (2017) 1138–1148. doi:10.1126/science.aab0530.

[41] L.M. Robeson, The upper bound revisited, J. Membr. Sci. 320 (2008) 390–400. doi:10.1016/j.memsci.2008.04.030.

[42] B. Comesaña-Gándara, J. Chen, C.G. Bezzu, M. Carta, I. Rose, M.C. Ferrari, E. Esposito, A. Fuoco, J.C. Jansen, N.B. McKeown, Redefining the Robeson upper bounds for CO_2/CH_4 and CO_2/N_2 separations using a series of ultrapermeable benzotriptycene-based polymers of intrinsic microporosity, Energy Environ. Sci. 12 (2019) 2733–2740. doi:10.1039/c9ee01384a.

[43] Y. Han, W.S.W. Ho, Polymeric membranes for CO_2 separation and capture, J. Membr. Sci. 628 (2021) 119244. doi:10.1016/j.memsci.2021.119244.

Figure Captions

Fig. 1. Schematic representation of the facilitated transport mechanisms.

Fig. 2. Chemical structures of carriers used for membrane synthesis.

Fig. 3. Schematic of the mixed-gas permeation measurement system.

Fig. 4. TGA curves of (a) PZEA, PZEA-Pro, and proline and (b) pure PVAm and a film containing 35 wt.% PVAm and 65 wt.% PEZA-Pro.

Fig. 5. FTIR spectra of pure PVAm, PZEA-Pro, and the PVAm blended with 65 wt.% PZEA-Pro.

Fig. 6. SEM cross-section image of membrane containing 35 wt.% PVAm and 65 wt.% PZEA-Pro after the gas permeation test.

Fig. 7. Experimental ellipsometric spectra and the corresponding model fittings of the composite membrane containing 35 wt.% PVAm and 65 wt.% PZEA-Pro at 25 °C and 1 atm.

Fig. 8. Comparisons of (a) CO_2 permeances and (b) CO_2/N_2 selectivities of the PVAm membranes with different AAS mobile carrier concentrations at 57 °C. Markers: PZEA-Lys (■); PZEA-Ala (●); PZEA-Pro (▲); PZEA-Sar (▼) [8]; PZEA-Pro/PZEA-Sar (65:20 wt./wt.) (♦).

Fig. 9. Photos of dried films of PVAm with various contents of PZEA-Pro and the PZEA-Pro salt.

Fig. 10. Stability of a FTM containing 65 wt.% PZEA-Pro, 20 wt.% PZEA-Sar, and 15 wt.% PVAm for a 110 h at 57 °C.

Fig. 11. CO_2/N_2 separation performances of the FTMs in this work vs. the 2008 Robeson upper bound [41] and the 2019 revised upper bound [42] assuming a membrane thickness of 170 nm.

Supporting information for

CO_2-selective membranes containing amino acid salts for CO_2/N_2 separation

Zhien Zhang [a], Shraavya Rao [a], Yang Han [a], Ruizhi Pang [a], W.S. Winston Ho [a,b,*]

[a] *William G. Lowrie Department of Chemical and Biomolecular Engineering, The Ohio State University, 151 West Woodruff Avenue, Columbus, OH 43210, USA*

[b] *Department of Materials Science and Engineering, The Ohio State University, 2041 College Road, Columbus, OH 43210, USA*

* Corresponding author. Tel.: +1 614 292 9970; fax: +1 614 292 3769.

E-mail address: ho.192@osu.edu (W.S.W. Ho).

TGA analysis of the membranes

Fig. S1 shows the TGA curves of PVAm blended with (1) 65 wt.% PZEA-Lys, (2) 65 wt.% PZEA-Ala, and (3) 65 wt.% PZEA-Pro and 20 wt.% PZEA-Sar. All three curves showed a minor weight loss due to the desorption of water and no thermal degradation was observed until 110 °C.

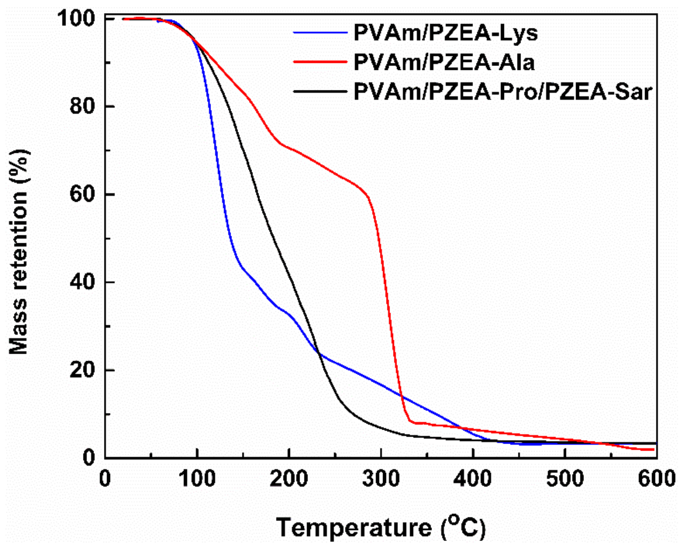

Fig. S1. FTIR spectra of PVAm blended with PZEA-Lys, PZEA-Ala, and PZEA-Pro/PZEA-Sar.

FTIR characterization of the membranes

Fig. S2 presents the FTIR spectra of PVAm blended with (1) 65 wt.% PZEA-Lys, (2) 65 wt.% PZEA-Ala, and (3) 65 wt.% PZEA-Pro and 20 wt.% PZEA-Sar. These peaks in the FTIR spectra were similar to PVAm/PZEA-Pro as indicated in Fig. 5.

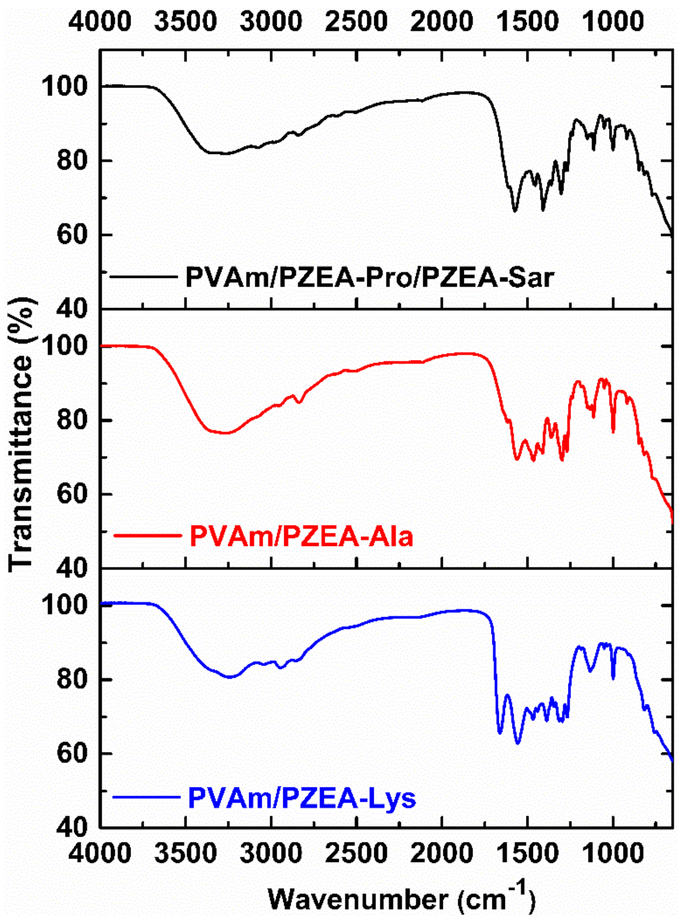

Fig. S2. FTIR spectra of PVAm blended with PZEA-Lys, PZEA-Ala, and PZEA-Pro/PZEA-Sar.

Effect of amine concentration on membrane performance

Fig. S3 demonstrates the effect of amine concentration on the transport results of the membranes. As seen, the membranes containing PZEA-Pro showed a better CO_2/N_2 separation performance albeit it had a higher MW and thus a lower amine concentration compared to other AAS carriers. Furthermore, PZEA-Ala and PZEA-Sar had similar molecular weights and hence similar amine molar concentrations; however, their transport performances differed significantly. Thus, the amine concentration was not a strong predictor of the membrane transport performance.

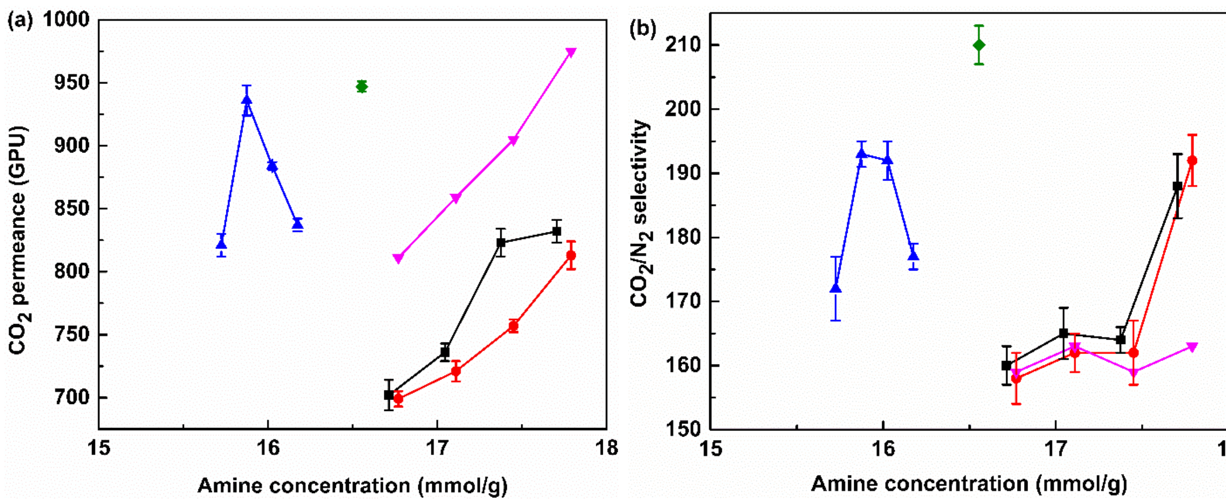

Fig. S3. Comparisons of (a) CO_2 permeances and (b) CO_2/N_2 selectivities of the PVAm membranes with different amine concentrations at 57 °C. Markers: PZEA-Lys (■); PZEA-Ala (●); PZEA-Pro (▲); PZEA-Sar (▼) [1]; PZEA-Pro/PZEA-Sar (65:20 wt./wt.) (♦).

Reference

[1] Y. Han, D. Wu, W.S.W. Ho, Nanotube-reinforced facilitated transport membrane for CO_2/N_2 separation with vacuum operation, J. Membr. Sci. 567 (2018) 261–271. doi:10.1016/j.memsci.2018.08.061.